

1 ~~Investigating the performance of Genetic Particle Filter in snow~~  
2 ~~data assimilation across snow climates~~ A genetic particle filter  
3 scheme for univariate data assimilation into Noah-MP model  
4 across snow climates

5 Yuanhong You<sup>a</sup>, Chunlin Huang<sup>b</sup>, Jinliang Hou<sup>b</sup>, Ying Zhang<sup>b</sup>

6  
7 <sup>a</sup>College of Geography and Tourism, Anhui Normal University, Wuhu, 241002, China

8  
9 <sup>b</sup>Northwest Institute of Eco-Environment and Resources, Chinese Academy of Sciences, Lanzhou,  
10 730000, China

11  
12  
13  
14  
15  
16 Corresponding author: Chunlin Huang, Key Laboratory of Remote Sensing of Gansu Province,  
17 Northwest Institute of Eco-Environment and Resources, Chinese Academy of Sciences, Lanzhou,  
18 Gansu, 730000, China. (huangcl@lzb.ac.cn)

19  
20  
21 Submitted to: Hydrology and Earth System Sciences

22 ~~October~~ March, 2022 ~~2023~~

## 24 Abstract

25 Accurate snowpack simulations are critical for regional hydrological predictions, snow  
26 avalanche prevention, water resource management, and agricultural production, particularly during  
27 the snow ablation period. Data assimilation methodologies are increasingly being applied to  
28 operational purposes to reduce the uncertainty in snowpack simulations and enhance their predictive  
29 capabilities. ~~With the aim of reducing the uncertainty of simulations, data assimilation methodology~~  
30 ~~is increasingly being applied in operational purposes.~~ This study aims to ~~investigate~~ investigates the  
31 feasibility of performance of using Genetic Particle Filter (GPF) ~~genetic particle filter which used as~~  
32 a snow data assimilation scheme, ~~designed~~ designed to assimilate ground-based snow depth (SD)  
33 measurements across different snow climates. We employed the default parameterization scheme  
34 combination within the Noah-MP model as the model operator in the snow data assimilation system  
35 ~~in the snow data assimilation system~~ to evolve snow variables and evaluated the assimilation  
36 performance of GPF using observational data from the sites with different snow climates. ~~– We also~~  
37 explored the impact of measurement frequency and particle number on the filter updating of the  
38 snowpack state at different sites and compared the results of generic resampling methods with the  
39 genetic algorithm used in the resampling process. ~~And the feasibility of genetic particle filter used as~~  
40 ~~snow data assimilation scheme was investigated at different sites, at the same time, the impact of~~  
41 ~~measurement frequency, particle number on the filter updating of the snowpack state were also~~  
42 ~~evaluated.~~ Our results demonstrated that the genetic particle filter GPF can be used as a snow data  
43 assimilation scheme to assimilate ground-based measurements and ~~obtain~~ obtain satisfactory  
44 assimilation performance ~~results~~ across different snow climates. We found that the particle number is  
45 ~~not the crucial factor to impact the~~ for the filter's performance, and ~~one hundred~~ 100 particles ~~can~~ are  
46 sufficient to represent the high dimensionality of the point-scale system. The frequency of  
47 measurements can significantly ~~affects~~ the filter updating performance, ~~of filter updating~~ and ~~a~~ dense  
48 ground-based snow observational data always ~~can~~ dominates the accuracy of assimilation results.  
49 Compared to generic resampling methods, the genetic algorithm used to resample particles can  
50 significantly enhance the diversity of particles and avoid particle degeneration and impoverishment.  
51 Finally, we concluded that the genetic particle filter GPF is a suitable candidate approach to snow data  
52 assimilation and is appropriate for different snow climates.

## 53 1. Introduction

54 Understanding snowpack dynamics is ~~of critical importance to~~ crucial for water resource  
55 management, agricultural production, avalanche prevention and flood preparedness in mountain area  
56 and flood predictions snow dominated regions (Piazzini et al., 2019; Pulliainen et al., 2020). As a special

57 ~~land surface type. The presence of~~ seasonal snow cover is highly sensitivity to climate change and  
58 has highly sensitivity to climate change and a great significant impact influence on energy and  
59 hydrological ~~eye~~processes (Barnett et al., 2005; Takala et al., 2011; Kwon et al., 2017; Che et al.,  
60 2014). ~~On one hand, the high~~High snow surface albedo can significantly reduce ~~the~~-shortwave  
61 radiation absorption, leading to adjustments in remarkably ~~and~~-the energy exchange between the land  
62 surface and atmosphere ~~will be adjusted~~ (You et al., 2020a; You et al., 2020b). ~~Moreover~~On the other  
63 ~~hand~~, the ~~property of~~-low thermal conductivity of snow cover can insulate the underlying soil,  
64 ~~resulting in reduced~~ whose temperature variability is severely reduced towards ~~and more~~ a stable  
65 conditions (Zhang et al., 2005; Piazzi et al., 2019). ~~Additionally, snowmelt~~Snowmelt is an important  
66 water resource ~~and that~~ plays a critical role in ~~water supply in terms of~~ soil moisture, runoff, and  
67 groundwater recharge (Dettinger, 2014; Griessinger et al., 2016; Oaida et al., 2019). Consequently,  
68 ~~succeeds~~understanding ~~in catching~~-snow dynamics is crucial ~~for predicting snowmelt runoff, for~~  
69 ~~snowmelt runoff~~, atmospheric circulation, ~~and~~-hydrological predictions, ~~and~~ climate change.

70 ~~Recently~~Currently, there is a growing effort ~~is aimed at to~~ investigating ~~investigate~~ the potential  
71 of data assimilation (DA) schemes ~~in consistently to improve~~improving snow simulations and obtain  
72 the optimal posterior estimate of ~~the~~ snowpack state (Bergeron et al., 2016; Piazzi et al., 2018; Smyth  
73 et al., 2020; Abbasnezhadi et al., 2021). ~~Many~~-Various different DA methodologies ~~with different~~  
74 ~~degrees of complexity~~ have been developed, ~~with distinct degree of complexity, certainly, various~~  
75 ~~performance since diverse level of complexity, resulting in diverse performance levels.~~ Sequential DA  
76 ~~techniques, including basic direct insertion, optimal interpolation schemes, ensemble-based Kalman~~  
77 ~~filter, and particle filter, have been widely employed in real-time applications. The greatest strength~~  
78 ~~of sequential DA techniques is that the model state can be sequentially updated when observational~~  
79 ~~data become available (Piazzi et al., 2018).~~The sequential DA techniques ~~including basic direct~~  
80 ~~insertion, optimal interpolation schemes, Kalman filter and its variants and particle filter are widely~~  
81 ~~employed in practical applications. The greatest strength of sequential DA technique is that the model~~  
82 ~~state can be sequentially updated when observational data available (Piazzi et al., 2018).~~However,  
83 ~~the direct insertion method, which replaces model predictions with observations when available, is~~  
84 ~~based on the assumption that the observation is perfect and the model prior is wrong (Malik et al.,~~  
85 ~~2012).~~ This method can potentially result in model shocks due to physical inconsistencies among  
86 ~~state variables (Magnusson et al., 2017).~~ The basic direct insertion method ~~simple~~ replace the model  
87 ~~predictions with observations when available on the assumption that the observation is perfect and~~  
88 ~~model prior is wrong (Malik et al., 2012).~~ However, this method possible result in model shocks due  
89 ~~to physical inconsistencies among state variables (Magnusson et al., 2017).~~ Although the optimal  
90 interpolation ~~method is more advanced scheme~~and takes into account ~~the~~-observational uncertainty,  
91 ~~it still this method still~~ has great limitations ~~and is rarely used in real-time operational systems~~ (Dee  
92 et al., 2011; Balsamo et al., 2015).-

93 ~~More advanced~~At a higher level are the Kalman filter and ~~its variants~~ensemble-based Kalman  
94 ~~filter~~, which are ~~typical sequential DA techniques and~~ most commonly used in various ~~real-time~~  
95 ~~applications. The standard Kalman filter (KF) just can be used in linear dynamic models since it~~  
96 ~~depends on the assumption of system linearity (Gelb, 1974).~~The Ensemble Kalman Filter (EnKF),  
97 ~~which was first introduced by Evensen in 2003, uses a Monte Carlo approach to approximate error~~  
98 ~~estimates based on an ensemble of model predictions. Ensemble Kalman filter (EnKF) was proposed~~  
99 ~~by Evensen (2003), in this method, the Monte Carlo approach was used to approximate error estimates~~  
100 ~~based on an ensemble of model simulations and this~~ This approach method does not require a model  
101 ~~a model~~ linearization, making it particularly advantageous. Precisely due to this advantage, the EnKF  
102 has been widely used in ~~snow data assimilations~~snowpack prediction. For example, ~~the EnKF has been~~  
103 ~~used was employed~~ to assimilate MODIS snow cover extent and AMSR-E SWE into a hydrologic  
104 model to improve modeled SWE (Andreadis et al., ~~2005~~2006), as well as to assimilate MODIS  
105 ~~fractional snow cover into a land surface model (Su et al., 2008). Moreover, the EnKF method has~~  
106 ~~been used to enhance snow water equivalent estimation by assimilating ground-based snowfall and~~  
107 ~~snowmelt rates, simultaneous assimilation of D-InSAR, automatically and manually measured snow~~  
108 ~~depth data (Yang and Li, 2021).~~The feasibility of assimilating fractional snow cover detected by  
109 MODIS into land surface model using EnKF was investigated, and the results show that the SWE  
110 estimates from the EnKF are most improved in various regions (Su et al., 2008). The impact of an  
111 ~~EnKF-based assimilation of both ground-based SWE observations and snowfall and snowmelt rates~~  
112 ~~on distributed SWE estimates was analyzed in Magnusson et al. (2014). More recently, three kinds of~~  
113 ~~snow depth data which included the D-InSAR data retrieved from the remote sensing images, the~~  
114 ~~automatically measured data using ultrasonic snow depth detectors, and the manually measured data~~  
115 ~~were assimilated based on ensemble Kalman filter, and the results demonstrated that the assimilated~~  
116 ~~snow depth data were spatiotemporally consecutive and integrated (Yang and Li, 2021). Although~~  
117 ~~Even though there are numerous the EnKF was widely used in snow data assimilation and many~~  
118 studies generally stated that the EnKF has an excellent assimilation performance enabling to  
119 consistently improve snow simulations, some constraining limitations hinder ~~the~~ filter performance  
120 (Chen, 2003). ~~One of the main limitations is that the EnKF assumes that the model states follow a~~  
121 ~~Gaussian distribution and only considers the~~ Firstly, this method was implemented at the assumption  
122 ~~of model states follow gaussian distribution and just considers the first and second order moments,~~  
123 ~~thereby losing relevant information contained in higher-order moments~~ higher-order moments be  
124 ~~ignored will makes relevant information be lost~~ (Moradkhani et al., 2005). Unfortunately, the dynamic  
125 systems are usually ~~has strongly nonlinearity~~ nonlinear and the involved probability distribution of  
126 ~~system~~ state variables are not supposed to follow a Gaussian distribution (Weerts and El Serafy, 2006).  
127 ~~Additionally~~Moreover, the filter performance ~~of the EnKF is~~ was significantly ~~affected~~ influenced by  
128 ~~the~~ linear updating procedure ~~in~~ EnKF, and the state-averaging operations can be particularly

129 ~~challenging may be a huge challenge~~ for highly ~~detailed~~ complex ~~snowpack~~ models.

130 ~~In order to overcome these limitations, the particle~~Partiele filter (PF) ~~which also based on Monte~~  
131 ~~Carlo method hasis been~~ developed for non-Gaussian, nonlinear dynamic models (Gordon et al.,  
132 ~~1993). based on sequential Monte Carlo and widely used in snow data assimilation in recent years~~  
133 ~~(Gordon et al., 1993).~~The greatest strength of PF ~~seheme-technique~~ is free from the constraints of  
134 model linearity and error following Gaussian distribution, ~~whichthis~~ makes the PF ~~techniqueseheme~~  
135 ~~succeed applied insuitable for~~ nonlinear and non-Gaussian dynamic systems. ~~This is also a significant~~  
136 ~~advantage of PF over than other assimilation algorithms.~~Additionally, PF ~~sehemes-technique~~ give  
137 weights to individual particles but leave model states untouched, ~~this-which~~ makes PF more  
138 computationally efficient than ensemble ~~Kalman-Kalman~~ filter and smoother (Margulis et al., 2015).  
139 ~~Thanks to these advantages, An-an~~ increasing interest focuses on applying PF ~~seheme-technique~~ in  
140 snow data assimilation. For example, remotely sensed microwave radiance data was assimilated into  
141 snow model for updating model states by PF ~~seheme-technique~~, and the results demonstrated that the  
142 SWE simulations have great improvement (Dechant and Moradkhani, 2011; ~~Deschamps-Berger et al.,~~  
143 ~~2022~~). A newly PF approach proposed by Margulis et al. (2015) was used to improve SWE estimation  
144 through assimilating remotely sensed fractional snow-covered area. ~~At basin scale, This-PF~~ technique  
145 was ~~also~~-implemented with the objective of obtaining high resolution retrospective SWE estimates  
146 ~~over several Andean study basins~~ (Cortes et al., 2016). ~~The PF~~ ~~techniqueseheme~~ was also used to  
147 assimilate daily snow depth observations within a multi-layer energy-balance snow model, ~~and result~~  
148 ~~in an improvement of to improve~~ SWE and snowpack runoff simulations ~~during the entire analysis~~  
149 ~~period~~ (Magnusson et al., 2017). Above studies ~~demonstrated that generally state that the PF seheme~~  
150 ~~is a well-performing data assimilation technique enabling to consistently improve model simulations.~~  
151 ~~And either the assimilation of assimilated the~~ snow-related in-situ measurements or remotely sensed  
152 ~~images-observation data~~ through PF ~~seheme-technique~~ can ~~successfullysueceeds in updatingupdate~~  
153 the predictions of snowpack dynamics, ~~and the PF seheme is a well-performing data assimilation~~  
154 ~~technique enabling to consistently improve model simulations.~~ Nevertheless, particle degeneracy is  
155 ~~still onthe~~ potential limitation for PF ~~techniqueseheme~~, it occurs when ~~the majoritymost~~ of particles  
156 have negligible weight and only ~~a small number of few~~ particles ~~with-have~~ significant weights, ~~such~~  
157 ~~thatwhich~~ makes the state probability distribution cannot be represented by the particles ~~loss their~~  
158 ~~ability to represent the state probability density function~~ (Parrish et al., 2012; Abbaszadeh et al., 2017;  
159 ~~Abbaszadeh et al., 2018~~). ~~The particle resampling has been considered to be an efficient approach~~  
160 ~~which can effectively mitigate the degeneracy problem, however, it may lead to the resulting sample~~  
161 ~~will contain many repeated points and a lack of diversity among the particles, which is defined sample~~  
162 ~~impoverishment~~ (Rings et al., 2012; Zhu et al., 2018). ~~Despite the resampling approach can effectively~~  
163 ~~mitigate the particle degeneracy phenomenon, another potential limitation has been the sample~~  
164 ~~impoverishment, that is, few particles have significant weight while most other particles with~~

165 ~~ignorable weight are abandoned during the resampling process, and the diversity of particles has been~~  
166 ~~reduced. And the sample impoverishment was a tricky problem for generic resampling methods.~~  
167 ~~Using intelligent search and optimization methods to mitigate the degeneracy problem may be a good~~  
168 ~~choice since it can avoid the sample impoverishment well (Park et al., 2009; Ahmadi et al., 2012;~~  
169 ~~Abbaszadeh et al., 2018).~~ The Genetic Algorithm (GA) as an intelligent search and optimization  
170 method has been ~~known as an effective approach to mitigate the degeneracy problem and received~~  
171 ~~more attention~~ employed to mitigate the degeneracy and impoverishment problem (Kwok et al., 2005;  
172 Park et al., 2009; Mechri et al., 2014). ~~GA is known as an effective approach to improve the~~  
173 ~~performance of particle filter and has received more attention.~~ The GA applied in particle filter, which  
174 ~~is defined genetic particle filter (GPF), has been successfully implemented to estimate parameters or~~  
175 ~~states in nonlinear models (Van Leeuwen, 2010; Snyder, 2011).~~ The GPF was also used as data  
176 ~~assimilation scheme applied to land surface model which simulates prior subpixel temperature and~~  
177 ~~the results showed the GPF outperformed prior model estimations (Mechri et al., 2014).~~ For example,  
178 ~~the crossover operator within GA was performed on the prior particles (Kwok et al., 2005).~~ Mechri  
179 ~~et al. (2014) implemented the genetic particle filter as data assimilation scheme and applied to land~~  
180 ~~surface model which simulates prior subpixel temperature, the results demonstrated that GPF~~  
181 ~~outperforms prior model estimations.~~ Despite a series of studies have proved that the GPF is an  
182 ~~effective data assimilation approach, however~~ However, few studies have ~~used~~ investigated the  
183 ~~performance of GPF as a snow data assimilation scheme, especially in different snow climates.~~  
184 ~~Certainly, in~~ In view of the promising performances of GPF ~~assimilation scheme in a~~ snow data  
185 ~~assimilation scheme,~~ this paper aims to investigate the potential of GPF in performing snow data  
186 assimilation, and the main goal of this research is to address the following issues: (1) Can the GPF  
187 be employed as a snow data assimilation scheme? (2) How is the assimilation performance of GPF  
188 in snow data assimilation across different snow climates? (3) The sensitivity of DA simulations to the  
189 frequency of the assimilated measurements and the particle number.

190 This paper is organized as follows. Section 2 ~~describes-introduces~~ the information of ~~observation~~  
191 ~~study sites, the meteorological dataset, the snow module within the Noah-MP model, calculation flow~~  
192 ~~of GPF DA-scheme, and DA-design of numerical experimental-design.~~ Section 3 explains the  
193 ~~simulation results of SD by open-loop ensemble, explores the sensitivity of measurement frequency~~  
194 ~~and ensemble size.~~ Experimental results are presented and discussed in Section 3. Section 4  
195 summarizes the findings of this study.

## 196 2. Materials and methods

### 197 2.1 Study sites and data

198 With the consideration of the filtering performance maybe ~~different under different~~

199 ~~environments diverse in snow climates, we selected~~ eight seasonally snow-covered study sites with  
 200 different snow climates in total ~~were selected to implement numerical experimental~~ in this study  
 201 (Sturm et al., 1995; Trujillo and Molotch, 2014). These sites are distributed at different latitudes in  
 202 the northern hemisphere, and the sites included the Arctic Sodankylä site (SDA, 179 m), located  
 203 beside the Kitinen River in Finland and has a 2 m depths soil frost (Rautiainen et al., 2014); the  
 204 Snoqualmie site (SNQ, 921 m) with a rain-snow transitional climate in the Washington Cascades of  
 205 the USA, in this site, the ~~snow depthSD~~ measured from snow stakes was employed (Wayand et al.,  
 206 2015); the maritime Col de Porte (CDP, 1330 m) site in the Chartreuse Range in the Rhone-Alpes of  
 207 France; the Mediterranean climate Refugio Poqueira site (ROPA, 2510 m) in Sierra Nevada  
 208 Mountains of Spain and has a high evaporation rate (Herrero et al., 2009); the Weissfluhjoch site  
 209 (WFJ, 2540 m) in Davos of Switzerland, and automatic observations of ~~snow depthSD~~ were used in  
 210 this study (Wever et al., 2015); the continental Swamp Angel Study Plot (SASP, 3370 m) site in the  
 211 San Juan Mountains of Colorado, USA; and two sites from typical snow-covered regions in China,  
 212 the Altay meteorological observation site (ATY, 735.3 m) in Northern Xinjiang, China, which has less  
 213 wind in the winter season; the other one is the Mohe meteorological observation site (MOHE, 438.5  
 214 m) in a county of Northeast China, which is the northernmost part of China and has a cold temperate  
 215 continental climate. Serially complete meteorological measurements are available and can be used as  
 216 forcing data in these sites, certainly, the downward longwave and shortwave radiation values of  
 217 MOHE were extracted from the China Meteorological Forcing Dataset (CMFD) (Chen et al, 2011),  
 218 since there are no radiation measurements in this site.

219 It is noteworthy that the spatial variance on the performance of the model is negligible since  
 220 these sites themselves are flat and surrounding vegetation types are uniform. We have used this data  
 221 set to examine the sensitivity of ~~snow depthSD~~ to physics options, and the results showed that the  
 222 dataset has a reliable quality. ~~in~~ In addition, the location, detailed information of snow climates, and  
 223 dataset process introduction of the eight sites can be also referenced in You et al. (2020a).

## 224 2.2 Snow module within Noah-MP model

225 The snow partial within Noah-MP model can be divided into three layers at most according to  
 226 snow depth (Yang et al., 2011). The SD  $h_{snow}$  is calculated by

$$227 \quad h_{snow}^t = h_{snow}^{t-1} + \frac{P_{s,g}}{\rho_{sf}} dt \quad (1)$$

228 where  $P_{s,g}$  is the snowfall rate at the ground surface,  $dt$  is the timestep, and  $\rho_{sf}$  is the bulk  
 229 density of the snowfall. When the snow depth  $h_{snow} < 0.025$  m, the snowpack is combined with the top

230 soil layer and there are no dependent snow layer exists. When  $0.025 \leq h_{snow} \leq 0.05$  m, the snow layer is

- 设置了格式: 字体: (默认) Times New Roman, 小四
- 域代码已更改
- 设置了格式: 字体: (默认) Times New Roman, 小四
- 带格式的: 右, 缩进: 首行缩进: 0 字符
- 域代码已更改
- 设置了格式: 字体: (默认) Times New Roman, 小四
- 设置了格式: 字体: (默认) Times New Roman, 小四
- 设置了格式: 字体: (默认) Times New Roman, 小四
- 设置了格式: 字体: (默认) Times New Roman, 小四
- 域代码已更改
- 域代码已更改
- 域代码已更改

231 created with the thickness equal to ~~snow-depthSD~~. When  $0.05 < h_{snow} \leq 0.1$  m, the snowpack will be  
 232 divided into two layers and both thickness  $\Delta z_{-1} = \Delta z_0 = h_{snow} / 2$ . When  $0.1 < h_{snow} \leq 0.25$  m, the thickness  
 233 of first layer is  $\Delta z_{-1} = 0.05$  m and the thickness of second layer is  $\Delta z_0 = (h_{snow} - \Delta z_{-1})$  m. When  
 234  $0.25 < h_{snow} \leq 0.45$  m, a third layer is created and the three thickness are:  $\Delta z_{-2} = 0.05$  m and  
 235  $\Delta z_{-1} = \Delta z_0 = (h_{snow} - \Delta z_{-2}) / 2$  m. When  $h_{snow} > 0.45$  m, the layer thickness of the three snow layers are  
 236  $\Delta z_{-2} = 0.05$  m,  $\Delta z_{-1} = 0.2$  m,  $\Delta z_0 = (h_{snow} - \Delta z_{-2} - \Delta z_{-1})$  m. Certainly, ~~the snow cover is highly~~  
 237 ~~influenced by air and ground temperature, the~~ snow layer is combined with the neighboring layer  
 238 since sublimation or melt, and be redivided depending on the total ~~snow-depthSD~~. The ~~snow module~~  
 239 ~~of Noah-MP~~ model provides an estimate of snow-related variables using energy and mass balance  
 240 which computing process requires a series of meteorological forcing data: ~~such as~~, near surface air  
 241 temperature, ~~wind speed and direction, relative humidity,~~ precipitation, ~~and air pressure,~~ downward  
 242 ~~solar longwave and shortwave~~ radiation. Snow accumulation or ablation parameterization of the  
 243 Noah-MP model is based on the mass and energy balance of the snowpack, and the snow water  
 244 equivalent can be calculated by following equation:

$$\frac{dW_s}{dt} = P_{s,g} - M_s - E \quad (24)$$

246 ~~Where where~~  $W_s$  is the snow water equivalent (mm),  $P_{s,g}$  is the solid precipitation ( $\text{mm s}^{-1}$ ),  $M_s$  is the  
 247 ~~snow ablation snowmelt~~ rate ( $\text{mm s}^{-1}$ ),  $E$  is the snow ~~evaporation sublimation~~ rate ( $\text{mm s}^{-1}$ ).

248 A snow interception model was implemented into Noah-MP model to describe the process of  
 249 ~~snowfall intercepted by the vegetation canopy (Niu and Yang, 2004). Due to the intereception of~~  
 250 ~~snowfall by the canopy and subsequent sublimation from the canopy snow can greatly reduce the~~  
 251 ~~quantity of snow falling on the ground, a snow interception model was implemented into Noah MP~~  
 252 ~~model~~. Within this model, the snowfall rate at the ground surface  $P_{s,g}$  is then calculated by

$$P_{s,g} = P_{s,drip} + P_{s,throu} \quad (3)$$

254 ~~where~~  $P_{s,drip}$  ( $\text{mm s}^{-1}$ ) is the drip rate of snow,  $P_{s,throu}$  ( $\text{mm s}^{-1}$ ) is the through-fall rate of snow. In  
 255 ~~Noah-MP model~~, the ground surface albedo is parameterized as an area-weighted average of albedos  
 256 of snow and bare soil, and the snow cover fraction of the canopy was used to calculate the ground  
 257 surface albedo. As in the equation (42),

$$\alpha_g = (1 - f_{snow,g}) \alpha_{soil} + f_{snow,g} \alpha_{snow} \quad (42)$$

设置了格式: 非突出显示

设置了格式: 字体: (默认) + 西文正文 (等线), 五号

设置了格式: 上标

设置了格式: 上标

设置了格式: 上标

域代码已更改

域代码已更改

设置了格式: 字体: (默认) Times New Roman, 小四

带格式的: 右, 缩进: 首行缩进: 0 字符

域代码已更改

设置了格式: 字体: (默认) Times New Roman, 小四

设置了格式: 字体: (默认) Times New Roman, 小四, 上标

设置了格式: 字体: (默认) Times New Roman, 小四

设置了格式: 字体: (默认) Times New Roman, 小四

设置了格式: 字体: (默认) Times New Roman, 小四, 上标

设置了格式: 字体: (默认) Times New Roman, 小四

带格式的: 缩进: 首行缩进: 0 字符

域代码已更改

域代码已更改



259 ~~Where~~  $\alpha_{soil}$  and  $\alpha_{snow}$  are the albedo of bare soil and snow, respectively.  $f_{snow,g}$  is the snow  
260 cover fraction on the ground and parameterized as a function of snow depth, ground roughness length  
261 and snow density (Niu and Yang, 2006).

### 262 2.3 Genetic particle filter data assimilation scheme

263 The Bayesian recursive estimation problem is solved by the Monte Carlo approach within PF  
264 technique, making this scheme is appropriate for nonlinear ~~models-system with~~ ~~and a non-~~  
265 ~~gaussian~~ ~~various~~ probability distributions (Magnusson et al., 2017). The ~~main-basic idea-concept~~ of  
266 PF technique is to use a large number of random realizations (i.e., particles) of the system state to  
267 represent the posterior distribution, ~~at the same time~~ ~~meanwhile~~, the particles are propagated forward  
268 in time as the model evolved. The weights associated with the particles are updated based on the  
269 likelihood of each particle's simulated proximity to the real observation, and the weight of the  
270 particles can be updated as follows:

$$271 \quad w_t^i = w_{t-1}^i p(z_t | x_t^i). \quad (35)$$

272 where  $w_{t-1}^i$  is the weight of  $i$ th particle at time  $t-1$  and the weight is updated by the likelihood  
273 function  ~~$p(z_t | x_t^i)$~~   ~~$p(z_t | x_t^i)$~~ , ~~which measures the likelihood of a given model state with respect to~~ the  
274 observation  $z_t$  ~~of state variable is employed in this function.~~ ~~Usually~~ ~~In general~~, a Gaussian ~~error~~  
275 distribution was ~~considered-assumed~~ to perturb the ~~observation values~~ ~~observations~~ and the likelihood  
276 function was defined to represent the errors. In this study, ~~we employed~~ a normal probability  
277 distribution ~~was employed~~ to serve as likelihood function:

$$278 \quad p(z_t | x_t^i) = N(z_t - x_t^i, \sigma). \quad (46)$$

279 ~~Where~~  $N$  ~~is-represents~~ the normal probability distribution of the residuals between ~~the~~  
280 observed,  $z_t$ , and simulated,  $x_t$ . Finally, the weights of the updated ~~model state-variable~~ would be  
281 normalized, and the assimilated value of ~~model state variable~~ is the weighted average of all particles  
282 at time  $t$ . Although the particle filter has ~~a broad vision of application been widely applied in various~~  
283 nonlinear systems, the particle degeneracy and impoverishment ~~in particle filter~~ are still the ~~fatal~~  
284 limitations ~~of particle filter need to be urgently addressed.~~ To ~~overcome-address~~ the degeneration  
285 problem in ~~the-PF technique~~ ~~algorithm~~, ~~the-traditional~~ resampling methods like multinomial  
286 resampling, systematic resampling, ~~etc.~~ were ~~used-employed~~ to resample the particles if the effective  
287 sample size,

$$288 \quad N_{eff} = 1 / \sum_{i=1}^N (w_t^i)^2. \quad (57)$$

289 fell below a specified number ~~of particles.~~ ~~To be honest, the traditional resampling methods can~~

带格式的: 缩进: 首行缩进: 0 字符

域代码已更改

带格式的: 缩进: 首行缩进: 0 字符

effectively mitigate the Although the particle degeneracy problem can be eliminated by the resampling methods resampling high-quality particles, however, it will ean also makeleads to the particles lack of diversity seriously after multiple iterations, that is the so-called particle impoverishment problem. For the sake of mitigating these two problems simultaneously, we employed theIn this study, the genetic algorithm (GA) was chosen to resample the particles, and this is the genetic particle filter algorithm (GPF). The GA was inspired by Darwin's evolution theory and emphasizes the principle of the survival of the fittest, exactly in fact, the "fitness"fitness\_ of particles should be chosen\_reselected in the partiele-filteringresampling phase according to the theory of particle filter. The selection, crossover and mutation are major steps to simulate population evolution, as shown in Figure 1, we used the three operators to produce better offspring and improve the whole population fitness, which was expected to prevent particle degeneracy and impoverishment. These three operators will be used to improve the particle fitness when the fitness less than a threshold value. The three operators are described as below.

**Selection mechanism:** At the time of assimilation, the selection operator will preferentially select the particles which close to the observed SD. This process is usually achieved by sorting the fitness value of all particles and selecting a certain proportion of particles. Here, we calculated the survival rate of all individuals and sorted them in ascending order, the top fifth percentile of particles were considered as high-quality particles and were selected as parents in genetic algorithm. This can ensure the fitness individuals can be delivered to next generation group. The survival rate of particles can be calculated by following equation:

$$P(x_{t,i}) = \exp\left[-\frac{1}{R_k}(x_{t,i,k|k-1} - z_k)^2\right] \quad (8)$$

where  $R_k$  is the observation error at time  $k$ , 0.01 m was set in this study;  $z_k$  represents the observed SD.

**Crossover mechanism:** The purpose of crossover operator is to exchange some genes for two or more chromosomes in a specified way to form new individuals. GA mainly generates new individuals by this way, which also determines the capability of global search. In this study, the arithmetic crossover method was used to generate new individuals and play the role of crossover operator. Selecting two particles randomly from the resampled particle group and combining them linearly to form a new particle. Assumed the two selected particles are  $\{x_m, x_n\}$ , and the new particles were formed by following equations:

$$x'_m = \alpha x_m + (1 - \beta) x_n \quad (9)$$

$$x'_n = \beta x_n + (1 - \alpha) x_m \quad (10)$$

设置了格式: 字体: 加粗

设置了格式: 字体: (默认) Times New Roman, 小四  
域代码已更改

设置了格式: 字体: (默认) Times New Roman, 小四  
设置了格式: 字体: (默认) Times New Roman, 小四  
设置了格式: 字体: (默认) Times New Roman, 小四  
域代码已更改

域代码已更改  
域代码已更改  
域代码已更改  
设置了格式: 字体: (默认) Times New Roman, 小四  
设置了格式: 字体: 加粗

设置了格式: 字体: (默认) Times New Roman, 小四  
域代码已更改

设置了格式: 字体: (默认) Times New Roman, 小四  
设置了格式: 字体: (默认) Times New Roman, 小四  
设置了格式: 字体: (默认) Times New Roman, 小四  
域代码已更改

设置了格式: 字体: (默认) Times New Roman, 小四  
域代码已更改

322 where  $\alpha$ ,  $\beta$  are the empirical crossover coefficients, and  $\alpha = 0.45$ ,  $\beta = 0.55$  in this study. In  
323 order to ensure the diversity of particles, the new formed particles will be abandoned when the  
324  $x'_m = x'_n$  occurred, and the parent individuals will be re-selected from the particle group.

325 **Mutation mechanism:** The mutation in GA refers to replacing the gene values at some loci with  
326 other alleles to form a new individual. The mutation mechanism can be considered as a supplement  
327 to the crossover mechanism which can increase the diversity of the population. Assuming that the  
328 randomly selected particle from the crossed particle set is, the mutation operation is performed on the  
329 particle by the following equation:

$$330 \quad x'_k = x_k + \eta * Uniform \quad (11)$$

331 where  $Uniform$  refers a random number from uniform distribution,  $\eta$  is empirical coefficient and  
332 0.01 was set in this study.

333 And the crossover and mutation operator can be used to produce better offspring to improve the whole  
334 population fitness, this can prevent sample impoverishment or a lack of particle diversity, especially  
335 when the processing noise is low. As shown in Figure 1, the effective ensemble size  $E_T$  was used to  
336 measure the degeneracy of the PF algorithm. The GA algorithm will be used to improve whole  
337 particles when  $E_T < E_0$ , and the procedure of GA can be divided into three steps: resample, crossover  
338 and mutation. First, the fitness of each particle was calculated and were then sorted in ascending order.  
339 Obviously, the fifth percentile of particles are fitness and be resampled. Second, the resampled  
340 particles were used to produce offspring by the crossover operator. Last, in order to increase the  
341 diversity of particles, the mutation operator was employed.

342 It is noteworthy that a large number of particles may lead to filter collapse (Meehri et al., 2014),  
343 here, we set the number of particles equals to 100 following references (Mechri et al., 2014;  
344 Magnusson et al., 2017; Piazzzi et al., 2018) in this study. Moreover, to avoid prevent the particle  
345 ensemble unable to represent the prior of state variable model state due to the model structurally  
346 deficient, a gaussian type model error,  $N(\mu, \sigma)$ , was added to the ensemble members. The  $\mu$  was  
347 obtained from the mean value of residual between simulation and observation, and the variance  $\sigma$   
348 was set to 0.01. deficient within model operator, in this study, a model error of gaussian noise type  
349 based on experience was added to the ensemble members before assimilating the measurements.

## 350 2.4 DA experimental design

### 351 2.4.1 Perturbation of meteorological input data

设置了格式: 字体: (默认) Times New Roman, 小四

设置了格式: 字体: (默认) Times New Roman, 小四

设置了格式: 字体: (默认) Times New Roman, 小四

设置了格式: 字体: (默认) Times New Roman, 小四

域代码已更改

域代码已更改

域代码已更改

域代码已更改

域代码已更改

设置了格式: 字体: (默认) Times New Roman, 小四

域代码已更改

设置了格式: 字体: (默认) Times New Roman, 小四

设置了格式: 字体: (默认) Times New Roman, 小四

设置了格式: 字体: (默认) Times New Roman, 小四

域代码已更改

域代码已更改

带格式的: 缩进: 首行缩进: 2 字符

设置了格式: 字体: (默认) Times New Roman, 小四

域代码已更改

域代码已更改

域代码已更改

352 The accuracy of model's output largely depends on the input meteorological forcing dataset for  
 353 land surface models, and meteorological forcing are one of the major sources of uncertainty affecting  
 354 simulation results (Raleigh et al., 2015). The precipitation and air temperature are the most important  
 355 input elements for snow simulations since their roles in determining the quantity of rainfall and  
 356 snowfall.

357 To produce the forcing data ensemble, the air temperature and precipitation were perturbed  
 358 following the method of Lei et al. (2014). In this study, the precipitation was assumed to have an error  
 359 with a log-normal distribution, and it is expressed as follows:

$$360 \quad P_t^i = \exp(\mu_{\ln P} + \varphi_{P,t} \cdot \sigma_{\ln P} / 2). \quad (612)$$

$$361 \quad \sigma_{\ln P} = \sqrt{\ln \left( \frac{(\alpha_p \cdot P_t)^2}{P_t^2} + 1 \right)}. \quad (713)$$

$$362 \quad \mu_{\ln P} = \ln \left( \frac{P_t^2}{\sqrt{P_t^2 + (\alpha_p \cdot P_t)^2}} \right). \quad (814)$$

363 Where  $P_t$  and  $P_t^i$  are the observed and perturbed precipitation at time  $t$ , respectively; the log  
 364 transformation of  $P_t^i$  is a Gaussian distribution with a mean ( $\mu_{\ln P}$ ) and a standard deviation ( $\sigma_{\ln P}$ );  
 365  $\alpha_p$  is the variance scaling factor of the precipitation, which was set to 0.5 in this study; and  $\varphi_{P,t}$  is  
 366 a normally distributed random number. ~~The number of particles was set to 100 according to the~~  
 367 ~~sensitivity experiment by Magnusson et al. (2017). Meanwhile, the~~The ensemble of the air  
 368 temperature was obtained as follows:

$$369 \quad T_t^i = T_t - \gamma(1 - 2w^i), w^i \sim U(0,1). \quad (915)$$

370 Where  $T_t$  and  $T_t^i$  are the observed and perturbed air temperatures at time  $t$ , respectively;  $\gamma$   
 371 is the variance scaling factor of the temperature with a value of 2.0; and  $w^i$  is the random noise with  
 372 a uniform distribution between 0 and 1. ~~An forcing ensemble containing 100 particles was obtained~~  
 373 ~~through above perturbation method in this study.~~

## 374 2.4.2 Evaluation metrics

375 In order to properly quantify the filter performance, each experiment is evaluated by statistical  
 376 analysis based on the daily mean values of simulations and observations. In this ~~paper~~study, we used  
 377 the ~~Kling-Gupta efficiency (KGE) coefficient (Gupta et al., 2009) to evaluate the filter performance,~~  
 378 ~~was evaluated using the Kling-Gupta efficiency (KGE) coefficient (Gupta et al., 2009) which~~ allows

379 the analysis of how the assimilation of snow observations succeeds in properly updating the model  
380 simulations, on average:

$$381 \quad KGE = 1 - \sqrt{(r-1)^2 + (a-1)^2 + (b-1)^2}. \quad (16)$$

382 Where  $r$  is the linear correlation coefficient between the simulated and observed SD;  $a$  is the  
383 ratio of the standard deviation of simulated SD to the standard deviation of the observed ones; and  $b$   
384 is the ratio of the mean of simulated SD to the mean of observed ones, ~~obviously here~~, the simulated  
385 SD is the mean SD ensemble simulations ~~in this paper~~. Theoretically, when  $r = 1$ ,  $a = 1$  and  $b = 1$   
386 in ~~formula equation (16)~~, the KGE will obtain the optimal value which ~~equal~~ to 1, ~~in this~~  
387 ~~case, and this illustrates that~~ the simulated SD highly consistent with the observed ones.

388 ~~To evaluate the performance of the assimilation, the~~ The time series of SD obtained from  
389 assimilation scenarios ~~is was~~ compared to observations ~~for evaluating the performance of the~~  
390 ~~assimilation~~, and the root-mean-square error (RMSE) was employed:

$$391 \quad RMSE = \sqrt{\frac{1}{N} \sum_{i=1}^N (obs(i) - sim(i))^2}. \quad (17)$$

392 Where  $N$  is the total number of observations,  $sim(i)$  is the simulated value at time  $i$ , and  
393  $obs(i)$  is the observed value at time  $i$ .

394 Another statistical index ~~employed as evaluation metric in this paper~~ is the continuous ranked  
395 probability skill score (CRPSS), ~~which is evaluated to assess changes to the overall accuracy of the~~  
396 ~~ensemble simulations of each experiment (CRPS) by considering the open-loop ensemble control run~~  
397 ~~as the reference one (CRPS<sub>ref</sub>)~~, and the calculation scheme is shown in ~~the following equation~~  
398 ~~formula~~ (18):

$$399 \quad CRPSS = 1 - \frac{CRPS}{CRPS_{ref}}. \quad (18)$$

400 Where ~~where~~ CRPS is the continuous ranked probability score which can ~~quantify measure~~ the  
401 difference between continuous probability distribution and deterministic observation samples (detail  
402 in Hersbach, 2000). A smaller CRPS value indicates better probabilistic simulation and the CRPS  
403 score of a perfect simulation would ~~equal equals~~ to 0. Therefore, the changes in overall accuracy of  
404 the SD ensemble simulations can be measured by CRPSS, ~~certainly~~ However, unlike the CRPS score,  
405 the optimal CRPSS score is equal to 1 and negative values indicate a negative improvement with  
406 respect to the reference ~~ones~~ control run.

### 407 3. Results and discussion

设置了格式: 字体: 小四  
域代码已更改

设置了格式: 字体: (默认) Times New Roman, 小四  
设置了格式: 字体: (默认) Times New Roman, 小四  
设置了格式: 字体: (默认) Times New Roman, 小四  
设置了格式: 字体: (默认) Times New Roman, 小四

域代码已更改

### 3.1 Open-loop ensemble simulations

To investigate the impact of meteorological perturbations on snow simulations, 400 an ensemble contained 100 snow depthSD simulations derived by as many different meteorological conditions were analyzed. For the sake of concision and clarity, we considered only 1 winter season for implementing snow simulation experiment at each site and the results were shown in Figure 2. For the sake of concision, a representative winter season was selected for each site and shown in Figure 2. As shown in Figure 2, the possible overestimation and underestimation of snow depthSD simulations produced by the perturbation forcing data were contained in the ensemble spread which are the direct consequence of perturbation of the forcing data. And the ensemble simulations are the direct consequence of perturbation of the forcing data. Certainly, since the meteorological perturbations are unbiased, the nonlinearity of physical processes within model is supposed to be the main reason for this issue under the condition of the meteorological perturbations are supposed to be unbiased the uncertainty (Piazzini et al. 2018). During the winter season in northern hemisphere, precipitation and air temperature are primary factors which can determine the total amount of snow. As Figure 2 shows, the intervals of SD ensemble are significant different in distinct at different sites though an identical meteorological perturbation method was used. In At some sites, like ATY, MOHE, WFJ and CDP, a larger SD ensemble interval spreads were obtained and most of SD observations were covered by the uncertainty spread ensemble spread, in this case, high-quality particles can be directly selected from the ensemble. However, in at some other sites, like in ROPA, SDA and SASP, a narrow SD ensemble interval spreads were obtained and the SD uncertainty spread interval of simulated SD can hardly cover the observations, in this case, the so-called high-quality particles even cannot be found in the ensemble and the model prior error become a prerequisite for succeed assimilation at this time. Especially at in ROPA site, the snow cover was extremely unstable with the result that we can hardly figure out any variation rules of snow depthSD, and the snow cover was extremely unstable. The narrow SD ensemble spread in these sites at this site also demonstrated that the precipitation and air temperature are were not the main factors causing snow change in these sites. Like in ROPA site According to literatures, sublimation losses at ROPA ranged from 24% to 33% of total annual ablation and occurred 60% of the time during which snow was present, and high sublimation rate may be the main reason for snow instability (Herrero et al., 2016; You et al., 2020a). This directly leads to a perfect ensemble spread which cover all observations cannot be produced by perturbing the air temperature and precipitation. Generally speaking, the ensemble produced by perturbing air temperature and precipitation does not contain high-quality particles at this site. It was found that the spread of SD ensembles is increased when a snowfall event occurred due to the perturbation in precipitation would providing different input snow rates for model realization at all sites. Despite this, we still found the simulated SD deviated from the observation seriously, like at SNQ site, the maximum value of simulated SD almost half of the maximum value of observed SD.

444 In this case, it is impossible to obtain a simulated SD ensemble spread which can cover or nearly  
445 cover the observation through perturbing the meteorological forcing data. At all sites, it was found  
446 that the spread of SD ensembles is increased when a snowfall event occurred due to the perturbation  
447 in precipitation would providing different input snow rates for model realization. It was expected to  
448 obtain a SD ensemble spread which can cover or nearly cover SD observations at all sites using the  
449 meteorological perturbation method, however, at some sites, like SNQ, SDA, etc., the spread of SD  
450 ensembles was found has a seriously underestimation. On the one hand, the precipitation and air  
451 temperature are not the dominant factors affecting snow cover change which lead to a narrowed  
452 ensemble spread at these sites. On the other hand, though the variation trend of snow cover can be  
453 accurately expressed by Noah-MP model, seriously underestimation of the simulated SD shows the  
454 snow simulation performance of Noah-MP is poor at these sites. Certainly, despite this Nonetheless,  
455 the simulated ensembles will be improved whenever the model and observation prior error of model  
456 state are is considered.

### 457 3.2 DA simulations with perturbed forcing data

458 Generally, the ability of a model to simulate autonomously can be limited if observation data is  
459 assimilated too frequently, resulting in assimilation results that are essentially the same as the  
460 observations and do not reflect the differences among models. To address this, In this study, the site  
461 SD measurements were assimilated into Noah-MP model and with an observation the frequency of  
462 SD observation is five 5 days in this study, enabling the GPF to perform differently at distinct sites.  
463 Figure 3 shows the The SD assimilation results across snow climates, indicating a substantial  
464 improvement in the SD simulations with satisfactory assimilation performance at all sites, are shown  
465 in Figure 3. It can be found that the GPF show a satisfactory assimilation performance at all sites, the  
466 SD simulations obtain a great improvement and closer to observations. Not only can the The GPF  
467 algorithm can handle not only algorithm solve the seriously underestimation, like such as at SNQ,  
468 SDA etc., but also the overestimation occurred during snow ablation period, such as seen at CDP,  
469 SASP, ATY and MOHE site, can be handled correctly. These results It was demonstrated demonstrate  
470 the effectiveness that of the GPF algorithm used as a snow data assimilation scheme and its ability to  
471 significantly can make a substantial improvement for improve SD simulations, despite the numerous  
472 seriously overestimations and underestimations that may occurred in the Noah-MP model's snow  
473 simulation results across snow climates.

474 With respect to the open loop run, the KGE values of the SD simulations relying on the perturbed  
475 meteorological forcing data reveal the effectiveness of GPF in updating SD simulations, The  
476 effectiveness of GPF in updating SD simulations is demonstrated by the KGE values of the DA  
477 simulations with perturbed meteorological forcing data, as shown in Figure 4. Although the mean  
478 ensemble simulations of SD show exhibit a substantial improvement at all sites, not all ensemble  
479 members were improved according to the distribution of KGE values as per the distribution of GPF-

480 DA KGE values. We found the ensemble members were actually obtained a substantial achieved  
481 significant improvement at some sites, like SDA, SASP, MOHE and SNQ, while others showed only  
482 and a slight improvement at sites like ATY, WFJ. However, Figure 4 also reveals that the update of  
483 SD model simulations at ROPA and WFJ sites are is more challenging. It was well known that the  
484 snowSnow simulation performance of Noah-MP model was poor at the ROPA site is known to be  
485 poor due to since the high sublimation rates special weather condition. Certainly, the median value of  
486 SD ensemble prediction KGE values as expected below zero at this site, indicating that there are few  
487 qualified simulations in the prediction ensemble. Even though the GPF succeeds in enhancing the SD  
488 simulations at ROPA site, the distribution of GPF-DA KGE values is not concentrated enough. The  
489 25th percentile approximately to 0.2 and the 75th percentile is about 0.7, more than half of ensemble  
490 members are below 0.5. This indicated that the GPF assimilation algorithm cannot enhance all  
491 members but it can raise the mean level and obtain an approximation of the optimal posterior  
492 estimation. While the GPF succeeds in enhancing the SD simulations at ROPA, the distribution of  
493 GPF-DA KGE values is not concentrated enough, with the 25th percentile approximately at 0.2 and  
494 the 75th percentile at about 0.7, indicating that the GPF assimilation algorithm cannot enhance all  
495 members but can raise the mean level and obtain an approximation of the optimal posterior estimation.  
496 Conversely, the assimilation of snow measurements at CDP site resulted in poor quality of the SD  
497 simulations compared to the open-loop ensemble simulations, the update of SD model predictions is  
498 more challenging at CDP site, and CDP is the only site which the assimilation of snow measurements  
499 actually results in a poor quality of the SD simulations with respect to the open-loop ensemble  
500 simulations. The median value of GPF-DA KGE was lower than the median value of OL KGE,  
501 indicating that a considerable number of ensemble simulations failed to capture the observed values  
502 after assimilating snow measurements. As shown in Figure 4, the median value of GPF-DA KGE is  
503 less than the median value of OL KGE, this indicates that a considerable number of ensemble  
504 simulations fail in well catching the observed values after assimilating snow data.  
505 Nevertheless, we still found Figure 3 shows that the mean ensemble simulations after  
506 assimilating snow data measurements are is much closer to SD observations in Figure 3. Thus, This  
507 explains it underscores the importance of that the ensemble mean in characterizing the filter  
508 effectiveness and the approximate is an important quantity to characterize the filter effectiveness and  
509 the practical value of the optimal posterior estimation of model state. Certainly, Additionally, the  
510 scale of the model ensemble spread was found to be is the determinant factor that which have a  
511 profound significantly affect effect on assimilation results. A large ensemble spread can adjust the  
512 simulations toward the observed system state even if the model predictions are heavily biased.

513 Figure 5 shows displays the CRPSS value of GPF-DA at different sites. The smaller the CRPSS  
514 value, the worst the probabilistic simulation (the optimal score being equal to 1). The highest CRPSS  
515 score of 0.91 was achieved at SASP, gets the maximum value 0.91, and while the lowest score is of

设置了格式: 非突出显示

设置了格式: 非突出显示

设置了格式: 非突出显示

设置了格式: 非突出显示

设置了格式: 非突出显示



516 0.44 was observed at CDP~~-site~~. ~~That-These results~~ indicates ~~that~~ the GPF enhances the overall  
517 accuracy of ~~the~~ ensemble simulations most at SASP~~-site~~ and least at CDP~~-site~~ with respect to the  
518 open-loop ensemble simulation. Certainly, this cannot be illustrated by the mean ensemble  
519 simulations (Figure 3) but consistent with the KGE statistical results (Figure 4). ~~Even~~  
520 ~~though~~~~Although~~ the open-loop simulations at SNQ ~~site show a very exhibited~~ ~~serious~~  
521 underestimation, a satisfactory assimilation result was obtained at this site ~~and the~~with a CRPSS score  
522 ~~is of~~ 0.87. At SNQ site, the snow simulation performance of Noah-MP model is poor and ~~the model~~  
523 shows ~~a a serious~~~~seriously~~ underestimation during snow stable phase, implementing data assimilation  
524 experiment in this case is a tricky business since it is ~~very~~ difficult to obtain a suitable simulated  
525 ensemble by perturbing the meteorological forcings. However, ~~due to~~since the model ~~prior error and~~  
526 ~~observation error are~~was considered in GPF algorithm, the overall accuracy of the ensemble  
527 simulations will be substantial enhanced and this ~~is~~ the reason why ~~it can obtain~~ a satisfactory  
528 assimilation result at SNQ site ~~can be obtained~~. ~~It is not easy to enhance the overall accuracy of the~~  
529 ~~ensemble simulations at ROPA, the ROPA was found to be a difficult site to enhance the overall~~  
530 ~~accuracy of ensemble simulations, with a CRPSS score of is only~~ 0.58, ~~at this site~~. The snow cover  
531 was ~~extremely highly~~ unstable and the variation ~~in of SD snow depth~~ exhibited extreme irregularity  
532 may be the main obstacles to snow data assimilation at this site.

533 Based on ~~the above analysis these findings~~, we concluded that the effectiveness of GPF varied  
534 among snow climates: it can be employed as snow data assimilation scheme across snow climates,  
535 however, it showed different performance at different sites. It is necessary to explore the sensitivity  
536 of measurement frequency and ensemble size ~~to for snow data~~GPF assimilation scheme ~~across for~~  
537 different sites.

### 538 3.3 Sensitivity analysis of DA scheme to SD measurement frequency

539 ~~For complex land/snow process models, model errors can gradually lead to the system deviating~~  
540 ~~from the true value. Therefore, it is necessary to continuously incorporate observations into the model~~  
541 ~~framework to adjust the operating trajectory of the state. Obviously, the frequency of incorporating~~  
542 ~~observations, that is, the assimilation interval, has an important impact on the assimilation system. To~~  
543 ~~investigate the effect of the SD measurement frequency on~~With the aim of investigating the  
544 performance of GPF ~~to SD measurement frequency~~, we conducted a ~~the~~sensitivity experiment was  
545 ~~conducted at the eight sites. We aimed to determine how reducing the frequency of SD measurements~~  
546 ~~affects the DA simulations. to assess how the reduction of SD observed data affects the DA~~  
547 ~~simulations. As expected, a decrease in SD measurement frequency led to a reduction in the impact~~  
548 ~~of the GPF updating on the model simulations, resulting in a gradual increase in the mean value of~~  
549 ~~RMSE. Obviously, a reduction in SD measurement frequency is expected to reduce the impact of the~~  
550 ~~GPF updating on the model simulations, and the RMSE mean value gradually increased. Figure 6~~  
551 ~~shows illustrates~~ the RMSE ensembles of ~~snow depth~~SD simulations resulting from ~~the~~

552 ~~assimilation~~assimilating of different frequency SD ~~observations~~measurements throughout over the  
553 snow period at all ~~sites~~each site. Higher frequency SD assimilation is beneficial in mitigating the  
554 RMSE value of simulated SD, as shown by the lower RMSE value achieved when the frequency of  
555 SD measurement was set to five days.Obviously, assimilating higher frequency of SD observations  
556 is more helpful to improve the effectiveness of GPF, like the frequency of SD observation equals to  
557 5 days, the ensemble simulations obtain lower RMSEs at all sites. This means that more frequent SD  
558 measurements improve the accuracy of the model, which is particularly useful in regions where snow  
559 conditions can change rapidly. The range of RMSE values at different sites varied significantly, as it  
560 was related to the maximum value of SD. For instance, a thick snow at SNQ and WFJ sites during  
561 the snow period led to larger RMSEs of SD simulations. Notably, an increase in the length of the  
562 assimilation window generally resulted in a significant increment of the RMSE value. However, an  
563 abnormal occurrence was observed at the SDA site, where the assimilation effect of 20 days of SD  
564 measurements was significantly better than that of 15 days. Although the RMSE distribution of SD  
565 assimilation results with 20 days of observations appeared superior to that of 15 days, the RMSE  
566 mean values of the two were very close: 0.08 m and 0.07 m, respectively. Therefore, this anomaly  
567 can be ignored. These results indicate that the frequency of SD observations has a significant impact  
568 on the effectiveness of the GPF algorithm and that dense observation data can effectively improve  
569 the assimilation result. Certainly, the range of RMSE values at different sites have a significant  
570 difference since it relates to the maximum snow depth, for instance, a thick snow at SNQ and WFJ  
571 site during the snow period lead to larger RMSEs of snow depth simulations. As shown in this figure,  
572 it is noteworthy that an increase in the length of assimilation window generally result in a significant  
573 increment of the simulation RMSE. Certainly, an abnormal situation occurred at SDA site, the  
574 assimilation effect of 20 days SD observations is significantly better than the assimilation effect of  
575 15 days SD observations. Actually, despite the RMSE distribution of SD assimilation result with 20  
576 days observations seems superior to the assimilation result with 15 days, however, the RMSE mean  
577 value of the two are very close, one is 0.08 m and the other is 0.07 m. Therefore, this anomaly can be  
578 ignored. It indicates that the frequency of SD observations has a significant impact on the  
579 effectiveness of GPF algorithm, and a dense observation data can effectively improve the assimilation  
580 result.

### 581 3.4 Sensitivity analysis of DA scheme to ensemble size

582 The ~~main~~results of the experiment ~~aiming~~aimed at to ~~evaluate~~evaluating the impact of particle  
583 number on the assimilation performance of GPF ~~is shown~~are presented in Figure 7. As expected, an  
584 ~~increase~~increasing in the particle number ~~which less than~~below the threshold ~~leads to~~generally result  
585 in a significant ~~increment~~improvement in of the percent effective sample size. However, the filter  
586 performance ~~is~~does not improve significantly ~~improved~~when the particle number ~~greater~~  
587 ~~than~~exceeds the threshold. Figure 7 shows that the GPF ~~algorithm yields~~would get the minimum

设置了格式: 字体: (默认) Arial, 四号, 倾斜

带格式的: 正文, 2 级, 缩进: 首行缩进: 0 厘米

588 error at all sites when the particle number is set to 100, and indicating that one hundred particles can  
589 optimize the performance of GPF algorithm. Although a large particle number can enhance particle  
590 diversity and prevent filter divergence, it will increase the computation burden without reducing,  
591 and this cannot reduce the error of the system. As shown-illustrated in Figure 7, the RMSEs are  
592 basically-generally at the same level when the particle number equals to 120 and 160, and the RMSE  
593 is-are significantly larger than the RMSE when the particle number is equal to 100. The slight impact  
594 of the change in the particle number on the performance of GPF, when the particle number is below  
595 the threshold, indicates low system sensitivity to the ensemble size, and this is observed at all sites. A  
596 low system sensitivity to the ensemble size is also clearly proven by the slight impact of the change  
597 in the particle number on the performance of GPF when the particle number is less than the threshold,  
598 and this has been occurred at all sites. Essentially, the increase of increasing the particle number  
599 blindly does not ensure-guarantee a better DA performance of the GPF algorithm. As shown  
600 demonstrated in Figure 7, although the particle number increased from 120 to 160, the RMSEs of  
601 simulated snow-depth are basically-virtually unchanged at all sites, despite an increase in the particle  
602 number from 120 to 160. It indicates This suggests that a-blindly increasing the ensemble size only  
603 increases the computational burden is futile to without improving the performance of GPF, it just can  
604 increase the computational burden.

### 605 3.5 Compared to traditional resampling methods

606 To demonstrate the effectiveness of using genetic algorithms for particle resampling, we  
607 compared the results of our genetic algorithm (PF-G) to those of traditional resampling methods:  
608 systematic resampling (PF-S) and multinomial resampling (PF-M), both of which are commonly used  
609 in particle resampling. The calculation process for these methods is detailed in the particle filter  
610 introduction references. Figure 8 shows the RMSE values of SD simulations using these three  
611 methods. We found that the PF-G outperforms PF-M and PF-S at all sites, as evidenced by the  
612 significantly smaller mean and median RMSE values. This indicates that the PF-G is suitable for  
613 snow data assimilation in different snow climates and is superior to traditional particle filters to a  
614 certain extent. At most sites (MOHE, ATY, SDA, and ROPA), PF-M and PF-S showed similar  
615 performance, meaning that these methods did not produce a significant difference in the assimilation  
616 results. This is because these traditional resampling methods can only address particle degeneration  
617 by resampling particles, but cannot prevent particle impoverishment. Therefore, they are unable to  
618 select high-quality particles and keep the particles have variety. Notably, the mean and median RMSE  
619 values for PF-G were significantly lower than those of PF-M and PF-S at some sites (SASP, SNQ,  
620 and WFJ) where the snow cover was relatively thick, with maximum SD during the snow period  
621 reaching 2.45 m, 2.95 m, and 2.40 m, respectively. This suggests that PF-G performs better in  
622 assimilating data from thick snow covers.

623 The multinomial and systematic resampling methods select particles from the original particle

624 set at different levels or based on the accumulation of particle weights. Both the two resampling  
625 methods extract particles from the entire particle set, and the corresponding particle values do not  
626 undergo any essential changes. However, compared with the two traditional particle resampling  
627 methods, genetic algorithm first uses the fitness function to calculate the "survival rate" of each  
628 particle one by one, and then performs crossover, mutation and other operations on the selected  
629 particles. This approach ensures that the resampled particles are high-quality particles, which is the  
630 main reason why genetic particle filtering has an advantage in the snow data assimilation experiments.  
631 As can be seen from Figure 8, the assimilation error by genetic particle filter is the smallest one at all  
632 sites. From the results of the real assimilation experiment, it can be seen that genetic particle filtering  
633 have more advantages over than other two methods.

## 634 4. Conclusions

635 This~~In this~~ study, we investigated the potential of using GPF ~~used~~ as a snow data assimilation  
636 scheme ~~across~~at eight sites ~~aeross~~-with varying different snow climates. ~~We addressed~~ ~~To solve~~ the  
637 problem of degeneration and impoverishment in PF algorithm by using the genetic algorithm to  
638 resample particles. ~~We also examined the sensitivity of GPF scheme to measurement frequency and~~  
639 ~~ensemble size. we used the genetic algorithm to resample particles when the particle threshold is~~  
640 ~~below 0.95. On this basis, we examined the sensitivity of GPF scheme to measurement frequency and~~  
641 ~~ensemble size.~~ The main findings of this study are as follows:-

- 642 1. The GPF was an effective snow data assimilation scheme and can be used across different snow  
643 climates. The genetic algorithm ~~ean~~-effectively ~~addressed~~~~solve~~ the problem of particle  
644 degeneration and impoverishment in PF algorithm.
- 645 2. ~~Our experiment showed that In this point-scale application of the ground SD measurement,~~ the  
646 system has ~~revealed~~ a low sensitivity to the particle number, ~~thereby proving that~~and 100 particles  
647 can ~~be obtained~~~~achieve~~ a better assimilation result across different snow climates, ~~that is,~~ This  
648 indicates that 100 particles ~~can be suited to~~are suitable for representing the high dimensionality  
649 of the system.
- 650 3. ~~The~~ We found that perturbations of the meteorological forcing data ~~has turn out not to be~~ were not  
651 sufficient ~~for to providing~~-provide ensemble spread, ~~and~~-resulting in a poor filter performance.  
652 ~~However,~~ ~~partiele~~Particle inflation can make up for this deficiency. ~~Moreover, we observed that~~  
653 ~~the~~The RMSE of simulated SD ~~would decreased~~~~decrease~~ significantly with the increase of the  
654 frequency of SD measurement, ~~that is,~~ indicating that a dense observational data can ~~dominate~~  
655 improve the assimilation results.
- 656 3.4. Compared to the two classic resampling methods, the particle filter with genetic algorithm as  
657 resampling method shows a better assimilation performance especially in a thick snow cover, the

658 ~~distribution RMSEs are more centralized and a smaller mean error will be obtained,~~  
 659 ~~The Our~~ experiments ~~conducted in this paper~~ were based on forcing data and snow observations from  
 660 ~~the various sites withaeross~~ different snow climates. ~~While our results provide a reference for~~  
 661 ~~applying GPF to snow data assimilation,~~ ~~On the one hand, the performance of the GPF on the regional~~  
 662 ~~scale is needed to be investigated; on the other hand, additional studies further research is are needed~~  
 663 ~~need to explore investigate the performance of GPF on a regional scale and to explore the assimilation~~  
 664 ~~ofthe~~ snow observational data ~~which~~ from remote sensing or wireless sensor ~~network networks~~  
 665 ~~assimilated into LSM land surface model~~ by GPF. ~~OverallIn~~ summary, our study demonstrates the  
 666 ~~results of this study providing a reference for applying the GPF to snow data assimilation and the~~  
 667 feasibility of ~~using GPF for snow data assimilation and provides valuable insights for future research~~  
 668 ~~in this area. across different snow climates has been proved.~~

## 669 Acknowledgements

670 This work was supported by the National Natural Science Foundation of China (grant number  
 671 42101361, 42130113, 41871251 and 41971326). ~~Key Research and Development Program of Anhui~~  
 672 ~~Province (2022107020028).~~

## 673 References

- 674 ~~Abbasnezhadi, K., Rousseau, A. N., Foulon, E., et al. and Savary, S.: (2021),~~ Verification of regional  
 675 deterministic precipitation analysis products using snow data assimilation for application in  
 676 meteorological network assessment in sparsely gauged Nordic basins, Journal of  
 677 Hydrometeorology, 22(4), 859-876, <https://doi.org/10.1175/JHM-D-20-0106.1>, 2021.
- 678 ~~Abbaszadeh, P., Moradkhani, H., Yan, H. X.: (2017),~~ Enhancing hydrologic data assimilation by  
 679 evolutionary particle filter and Markov Chain Monte Carlo, Advances in Water Resources, 111, 192-204,  
 680 <https://doi.org/10.1016/j.advwatres.2017.11.011>, 2018.
- 681 ~~Ahmadi, M., Mojallali, H., Izadi-Zamanabadi, R.: State estimation of nonlinear stochastic systems~~  
 682 ~~using a novel meta-heuristic particle filter, Swarm and Evolutionary Computation, 4, 44-53,~~  
 683 ~~<https://doi.org/10.1016/j.swevo.2011.11.004>, 2012.~~
- 684 ~~Andreadis, K. M., Lettenmaier, D. P.: Assimilating remotely sensed snow observations into a~~  
 685 ~~macroscale hydrology model, Advances in water resources, 29, 872-886, [https://doi.org/](https://doi.org/10.1016/j.advwatres.2005.08.004)~~  
 686 ~~[10.1016/j.advwatres.2005.08.004](https://doi.org/10.1016/j.advwatres.2005.08.004), 2006.~~
- 687 ~~Barnett, T. P., Adam, J. C., Lettenmaier, D. P.: (2005),~~ Potential impacts of a warming climate on  
 688 water availability in snow-dominated regions, Nature, 438(7066), 303-309, [https://doi.org/](https://doi.org/10.1038/nature04141)  
 689 ~~[10.1038/nature04141](https://doi.org/10.1038/nature04141), 2005.~~
- 690 ~~Balsamo, G., Albergel, C., Beljaars, A., Boussetta, S., Burun, E., Cloke, H., Dee, D., Dutra, E.,~~  
 691 ~~Munoz-Sabater, J., Pappenberger, F., de Rosnay, P., Stockdale, T., and Vitart, F.: et al. (2015),~~  
 692 ERA-Interim/Land: a global land surface reanalysis data set, Hydrology and Earth System

693 Sciences, 19(4): 389-407, <https://doi.org/10.5194/hess-19-389-2015>, 2015.

694 [Bergeron, J. M., Trudel, M., Leconte, R.: Combined assimilation of streamflow and snow water](#)  
695 [equivalent for mid-term ensemble streamflow forecasts in snow-dominated regions, Hydrology](#)  
696 [and Earth System Sciences, 20, 4375-4389, https://doi.org/10.5194/hess-20-4375-2016](#), 2016.

697 [Che, T., Li, X., Jin, R., and Huang, C. L.: Assimilating passive microwave remote sensing data into a](#)  
698 [land surface model to improve the estimation of snow depth, Remote Sensing of Environment,](#)  
699 [143, 54-63, https://doi.org/10.1016/j.rse.2013.12.009](#), 2014.

700 [Chen, Z.: ~~\(2003\)~~, Bayesian filtering: From Kalman filters to particle filters, and beyond, Adaptive](#)  
701 [Systems Laboratory Technical Report, McMaster University, Hamilton, 25pp., 2003, Statistics,](#)  
702 [182\(1\): 1-69.](#)

703 [Chen, Y. Y., Yang, K., He, J., Qin, J., Shi, J. C., Du, J. Y., and He, Q.: Improving land surface](#)  
704 [temperature modeling for dry land of China, Journal of Geophysical Research-Atmospheres,](#)  
705 [116, D20104, https://doi.org/10.1029/2011JD015921](#), 2011.

706 [Cortes, G., Giroto, M., Margulis, S.: ~~\(2016\)~~, Snow process estimation over the extratropical Andes](#)  
707 [using a data assimilation framework integrating MERRA data and Landsat imagery, Water](#)  
708 [Resources Research, 52,\(4\): 2582-2600, https://doi.org/10.1002/2015WR018376](#), 2016.

709 [Dee, D. P., Uppala, S. M., Simmons, A. J., Berrisford, P., Poli, P., Kobayashi, S., Andrae, U.,](#)  
710 [Balmaseda, M. A., Balsamo, G., Bauer, P., Bechtold, P., Beljaars, A. C. M., van de Berg, L.,](#)  
711 [Bidlot, J., Bormann, N., Delsol, C., Dragani, R., Fuentes, M., Geer, A. J., Haimberger, L., Healy,](#)  
712 [S. B., Hersbach, H., Holm, E. V., Isaksen, I., Kallberg, P., Koehler, M., Matricardi, M., McNally,](#)  
713 [A. P., Monge-Sanz, B. M., Morcrette, J. J., Park, B. -K., Peubey, C., de Rosnay, P., Tavolato, C.,](#)  
714 [Thepaut, J. N., and Vitart, F.: ~~et al. \(2011\)~~, The ERA-Interim reanalysis: configuration and](#)  
715 [performance of the data assimilation system, Quarterly Journal of the Royal Meteorological](#)  
716 [Society, 137\(656\): 553-597, https://doi.org/10.1002/qj.828](#), 2011.

717 [Dechant, C., Moradkhani, H.: ~~\(2011\)~~, Radiance data assimilation for operational snow and](#)  
718 [streamflow forecasting, Advances in Water Resources, 34\(3\): 351-364, https://doi.org/](#)  
719 [10.1016/j.advwatres.2010.12.009](#), 2011.

720 [Deschamps-Berger, C., Cluzet, B., Dumont, M., Lafaysse, M., Berthier, E., Fanise, P., Gascoin, S.:](#)  
721 [Improving the Spatial Distribution of Snow Cover Simulations by Assimilation of Satellite](#)  
722 [Stereoscopic Imagery, Water Resources Research, 58, https://doi.org/10.1029/2021WR030271,](#)  
723 [2022.](#)

724 [Dettinger, M.: ~~\(2014\)~~, Climate change impacts in the third dimension, Nature Geoscience, 7\(3\): 166-](#)  
725 [167, https://doi.org/10.1038/ngeo2096](#), 2014.

726 [Evensen, G.: The ensemble Kalman filter: Theoretical formulation and practical implementation,](#)  
727 [Ocean Dynamics, 53, 343-367, https://doi.org/10.1007/s10236-003-0036-9](#), 2003.

728 [Gelb, A.: ~~\(1974\)~~, Optimal linear filtering, in: Applied optimal estimation, MIT Press, Cambridge,](#)  
729 [Mass, 102-155, 1974.](#)

730 [Gordon, N. J., Salmond, D. J., Smith, A. F. M.: Novel-Approach to nonlinear non-Gaussian bayesian](#)  
731 [state estimation, IEE Proceedings-F Radar and Signal Processing, 140, 107-113, https://doi.org/](#)

设置了格式

732 [10.1049/ip-f-2.1993.0015](https://doi.org/10.1049/ip-f-2.1993.0015), 1993.

733 Griessinger, N., Seibert, J., Magnusson, J., and Jonas, T.: ~~et al.~~ (2016); Assessing the benefit of snow  
734 data assimilation for runoff modeling in Alpine catchments, *Hydrology and Earth System*  
735 *Sciences*, 20(9):, 3895-3905, <https://doi.org/10.5194/hess-20-3895-2016>, 2016.

736 [Gupta, H. V., Kling, H., Yilmaz, K. K., and Martinez, G. F.: Decomposition of the mean squared error  
737 and NSE performance criteria: Implications for improving hydrological modelling, \*Journal of\*  
738 \*Hydrology\*, 377, 80-91, <https://doi.org/10.5194/10.1016/j.jhydrol.2009.08.003>, 2009.](https://doi.org/10.5194/10.1016/j.jhydrol.2009.08.003)

739 [Herrero, J., Polo, M. J., Monino, A., and Losada, M. A.: An energy balance snowmelt model in a  
740 Mediterranean site, \*Journal of Hydrology\*, 371, 98-107, <https://doi.org/10.1016/j.jhydrol.2009.03.021>, 2009.](https://doi.org/10.1016/j.jhydrol.2009.03.021)

742 [Herrero, J., Polo, M. J., Pimentel, R., and Pérez-Palazón, M. J.: Meteorology and snow depth at  
743 Refugio Poqueira \(Sierra Nevada, Spain\) at 2510 m 2008-2015, PANGEA, 2016.](https://doi.org/10.1016/j.jhydrol.2009.03.021)

744 Hersbach, H.: ~~(2000)~~, Decomposition of the continuous ranked probability score for ensemble  
745 prediction systems, *Weather and Forecasting*, 15,(5): 559-570, [https://doi.org/10.1175/1520-0434\(2000\)015<0559:DOTCRP>2.0.CO;2](https://doi.org/10.1175/1520-0434(2000)015<0559:DOTCRP>2.0.CO;2), 2000.

747 Kwok, N., Fang, G., Zhou, W., ~~(2005)~~: Evolutionary particle filter: resampling from the genetic  
748 algorithm perspective. In: *Proceedings of International Conference on Intelligent Robots and*  
749 *Systems*, Shaw Conference Centre, Edmonton, Alberta, Canada, August 2-6, pp. 2935-2940,  
750 2005.

751 [Kwon, Y., Yang, Z. L., Hoar, T. J., and Toure, A. M.: Improving the radiance assimilation performance  
752 in estimating snow water storage across snow and land-cover types in North America, \*Journal\*  
753 \*of Hydrometeorology\*, 18, 651-668, <https://doi.org/10.1175/JHM-D-16-0102.1>, 2017.](https://doi.org/10.1175/JHM-D-16-0102.1)

754 [Meehri, R., Otle, C., Pannekouche, O., et al. \(2014\); Genetic particle filter application to land surface  
755 temperature downscaling, \*Journal of Geophysical Research Atmospheres\*, 119\(5\): 2131-2146.](https://doi.org/10.1029/2014JG002146)

756 [Lei, F. N., Huang, C. L., Shen, H. F., and Li, X.: Improving the estimation of hydrological states in  
757 the SWAT model via the ensemble Kalman smoother: Synthetic experiments for the Heihe River  
758 Basin in northwest China, \*Advances in Water Resources\*, 67, 32-45, <https://doi.org/10.1016/j.advwatres.2014.02.008>, 2014.](https://doi.org/10.1016/j.advwatres.2014.02.008)

760 [Malik, M. J., van der Velde, R., Vekerdy, Z., and Su, Z. B.: Assimilation of Satellite-Observed Snow  
761 Albedo in a Land Surface Model, \*Journal of Hydrometeorology\*, 13, 1119-1130, <https://doi.org/10.1175/JHM-D-11-0125.1>, 2012.](https://doi.org/10.1175/JHM-D-11-0125.1)

763 Magnusson, J., Gustafsson, D., Husler, F., ~~et al.~~ and Jonas, T.: (2014); Assimilation of point SWE data  
764 into a distributed snow cover model comparing two contrasting methods, *Water Resources*  
765 *Research*, 50(40):, 7816-7835, <https://doi.org/10.1002/2014WR015302>, 2014.

766 Margulis, S. A., Giroto, M., Cortes, G., ~~et al.~~ and Durand, M.: (2015); A particle batch smoother  
767 approach to snow water equivalent estimation, *Journal of Hydrometeorology*, 16(4):, 1752-1772,  
768 <https://doi.org/10.1175/JHM-D-14-0177.1>, 2015.

769 Magnusson, J., Winstral, A., Stordal, A. S., [Essery, R., and Jonas, T:et al. \(2017\); Improving  
770 physically based snow simulations by assimilating snow depths using the particle filter, \*Water\*](https://doi.org/10.1002/2017WR020888)

设置了格式: 非突出显示

设置了格式: 非突出显示

设置了格式: 非突出显示

设置了格式: 非突出显示

设置了格式: 非突出显示

设置了格式: 非突出显示

设置了格式: 非突出显示

设置了格式: 非突出显示

设置了格式: 非突出显示

设置了格式: 非突出显示

771 Resources Research, 53(2):, 1125-1143, <https://doi.org/10.1002/2016WR019092>, 2017.

772 Moradkhani, H., Hsu, K. L., Gupta, H., ~~et al.~~ and Sorooshian, S.: (2005), Uncertainty assessment of  
773 hydrologic model states and parameters: Sequential data assimilation using the particle filter,  
774 Water Resources Research, 41(5):, W05012, <https://doi.org/10.1029/2004WR003604>, 2005.

775 Mechri, R., Otle, C., Pannekoucke, O., and Kallel, A.: ~~et al.~~ (2014), Genetic particle filter application  
776 to land surface temperature downscaling, Journal of Geophysical Research-Atmospheres,  
777 119(5):, 2131-2146, <https://doi.org/10.1002/2013JD020354>, 2014.

778 Niu, G. Y., Yang, Z. L.: Effects of vegetation canopy processes on snow surface energy and mass  
779 balances, Journal of Geophysical Research-Atmospheres, 109, D23111, [https://doi.org/](https://doi.org/10.1029/2004JD004884)  
780 [10.1029/2004JD004884](https://doi.org/10.1029/2004JD004884), 2004.

781 Niu, G. Y., Yang, Z. L. (2006): Effects of frozen soil on snowmelt runoff and soil water storage at a  
782 continental scale, Journal of Hydrometeorology, 7(5):, 937-952, <https://doi.org/10.1175/JHM53>  
783 [8.1](https://doi.org/10.1175/JHM53), 2006.

784 Oaida, C. M., Reager, J. T., Andreadis, K. M., David, C. H., Levoe, S. R., Painter, T. H., Bormann, K.  
785 J., Trangsrud, A. R., Giroto, M., and Famiglietti, J. S.: et al. (2019), A high-resolution data  
786 assimilation framework for snow water equivalent estimation across the western United States  
787 and validation with the airborne snow observatory, Journal of Hydrometeorology, 20(3):, 357-  
788 378, <https://doi.org/10.1175/JHM-D-18-0009.1>, 2019.

789 Park, S., Hwang, J. P., Kim, E., and Kang, H. J.: ~~et al.~~ (2009). A new evolutionary particle filter for  
790 the prevention of sample impoverishment, IEEE Transaction on Evolutionary Computation,  
791 13(4):, 801-809, <https://doi.org/10.1109/TEVC.2008.2011729>, 2009.

792 Parrish, M. A., Moradkhani, H., DeChant, C. M.: (2012), Toward reduction of model uncertainty:  
793 Integration of Bayesian model averaging and data assimilation, Water Resources Research, 48:  
794 W03519, <https://doi.org/10.1029/2011WR011116>, 2012.

795 Piazzzi, G., Campo, L., Gabellani, S., Castelli, F., Cremonese, E., di Cella, U. M., Stevenin, H., and  
796 Ratto, S. M.: et al. (2019), An EnKF-based scheme for snow multivariable data assimilation at  
797 an Alpine site, Journal of Hydrology and Hydromechanics, 67(1):, 4-19,  
798 <https://doi.org/10.2478/joh-h-2018-0013>, 2019.

799 Piazzzi, G., Thirel, G., Campo, L., and Gabellani, S.: ~~et al.~~ (2018), A particle filter scheme for  
800 multivariate data assimilation into a point-scale snowpack model in an Alpine environment,  
801 Cryosphere, 12(7):, 2287-2306, <https://doi.org/10.5194/tc-12-2287-2018>, 2018.

802 Pulliainen, J., Luojus, K., Derksen, C., Mudryk, L., Lemmetyinen, J., Salminen, M., Ikonen, J., Takala,  
803 M., Cohen, J., Smolander, T., and Norberg, J.: Patterns and trends of Northern Hemisphere snow  
804 mass from 1980 to 2018, Nature, 581, 294-298, <https://doi.org/10.1038/s41586-020-2258-0>,  
805 [2020.](https://doi.org/10.1038/s41586-020-2258-0)

806 Rautiainen, K., Lemmetyinen J., Schwank, M., Kontu, A., Menard, C. B., Matzler, C., Drusch, M.,  
807 Wiesmann, A., Ikonen, J., and Pulliainen, J.: Detection of soil freezing from L-band passive  
808 microwave observations, Remote Sensing of Environment, 147, 206-218, [https://doi.org/10.101](https://doi.org/10.1016/j.rse.2014.03.007)  
809 [6/j.rse.2014.03.007](https://doi.org/10.1016/j.rse.2014.03.007), 2014.



810 [Raleigh, M. S., Lundquist, J. D., Clark, M.P.: Exploring the impact of forcing error characteristics on](#)  
811 [physically based snow simulations within a global sensitivity analysis framework, \*Hydrology\*](#)  
812 [and \*Earth System Sciences\*, 19, 3153-3179, <https://doi.org/10.5194/hess-19-3153-2015>, 2015.](#)

813 [Rings, J., Vrugt, J. A., Schoups, G., Huisman, J. A., and Vereecken, H.: Bayesian model averaging](#)  
814 [using particle filtering and Gaussian mixture modeling: Theory, concepts, and simulation](#)  
815 [experiments, \*Water Resources Research\*, 48, W05520, <https://doi.org/10.1029/2011WR011607>,](#)  
816 [2012.](#)

817 Smyth, E. J., Raleigh, M. S., Small, E. E. (2020): Improving SWE estimation with data assimilation:  
818 the influence of snow depth observation timing and uncertainty, *Water Resources Research*,  
819 56,(5): e2019WR026853, <https://doi.org/10.1029/2019WR026853>, 2020.

820 [Sturm, M., Holmgren, J., Liston, G. E.: A seasonal snow cover classification system for local to global](#)  
821 [applications, \*Journal of Climate\*, 8, 1261-1283, \[https://doi.org/10.1175/1520-0442\\(1995\\)008<1\]\(https://doi.org/10.1175/1520-0442\(1995\)008<1\)](#)  
822 [261:ASSCCS>2.0.CO;2, 1995.](#)

823 Su, H., Yang, Z. L., Niu, G. Y., and Dickinson, R. E.: (2008), Enhancing the estimation of continental-  
824 scale snow water equivalent by assimilating MODIS snow cover with the ensemble Kalman  
825 filter, *Journal of Geophysical Research-Atmospheres*, 113(D8):, D08120, <https://doi.org/10.1029/2007JD009232>, 2008.

827 [Snyder, C.: Particle filters, the optimal proposal and high-dimensional systems, \*ECMWF Seminar on\*](#)  
828 [Data Assimilation for Atmosphere and Ocean](#), pp. 6-9, Reading, U. K., 2011.

829 Takala, M., Luojus, K., Pulliainen, J., Derksen, C., Lemmetyinen, J., Karna, J. P., Koskinen, J., and  
830 [Bojkov, B.: et al. \(2011\), Estimating northern hemisphere snow water equivalent for climate](#)  
831 [research through assimilation of space-borne radiometer data and ground-based measurements,](#)  
832 [Remote Sensing of Environment](#), 115(12):, 3517-3529, <https://doi.org/10.1016/j.rse.2011.08.014>, 2011.

834 [Trujillo, E., Molotch, N.P.: Snowpack regimes of the Western United States, \*Water Resources\*](#)  
835 [Research](#), 50, 5611-5623, <https://doi.org/10.1002/2013WR014753>, 2014.

836 [Van Leeuwen, P. J.: Nonlinear data assimilation in geosciences: An extremely efficient particle filter,](#)  
837 [Quarterly Journal of the Royal Meteorological Society](#), 136, 1991-1999, <https://doi.org/10.1002/qj.699>, 2010.

839 [Wayand, N. E., Massmann, A., Butler, C., Keenan, E., Stemberis, J., and Lundquist, J. D.: A](#)  
840 [meteorological and snow observational data set from Snoqualmie Pass \(921 m\), Washington](#)  
841 [Cascades, USA, \*Water Resources Research\*, 51, 10092-10103, <https://doi.org/10.1002/2015WR017773>,](#)  
842 [2015.](#)

843 Weerts, A. H., El Serafy, G. Y. H.: (2006), Particle filtering and ensemble Kalman filtering for state  
844 updating with hydrological conceptual rainfall-runoff models, *Water Resources Research*, 42(9):,  
845 W09403, <https://doi.org/10.1029/2005WR004093>, 2006.

846 [Wever, N., Schmid, L., Heilig, A., Eisen, O., Fierz, C., and Lehning, M.: Verification of the multi-](#)  
847 [layer SNOWPACK model with different water transport schemes, \*The Cryosphere\*, 9, 2271-](#)  
848 [2293, <https://doi.org/10.5194/tc-9-2271-2015>, 2015.](#)

849 Yang, J. M., Li, C. Z.: ~~(2021)~~, Assimilation of D-InSAR snow depth data by an ensemble Kalman  
850 filter, *Arabian Journal of Geosciences*, 14(6):, 5051-14, <https://doi.org/10.1007/s12517-021-066>  
851 [99-y](https://doi.org/10.1007/s12517-021-066), 2021.

852 You, Y. H., Huang, C. L., Yang, Z. L., Zhang, Y., Bai, Y. L., and Gu, J.: Assessing Noah-MP  
853 parameterization sensitivity and uncertainty interval across snow climates, *Journal of*  
854 *Geophysical Research-Atmospheres*, 125, e2019JD030417, <https://doi.org/10.1029/2019JD030>  
855 [417](https://doi.org/10.1029/2019JD030), 2020.

856 Zhang, T. J. ~~(2005)~~: Influence of the seasonal snow cover on the ground thermal regime: An overview,  
857 *Reviews of Geophysics*, 43(4):, RG40024-23, <https://doi.org/10.1029/2004RG000157>, 2005.

858 Zhu, G. F., Li, X., Ma, J.Z., Wang, Y. Q., Liu, S. M., Huang, C. L., Zhang, K., and Hu, X. L.: A new  
859 moving strategy for the sequential Monte Carlo approach in optimizing the hydrological model  
860 parameters, *Advances in Water Resources*, 114, 164-179, <https://doi.org/10.1016/j.advwatres>.  
861 [2018.02.007](https://doi.org/10.1016/j.advwatres), 2018.

862

863

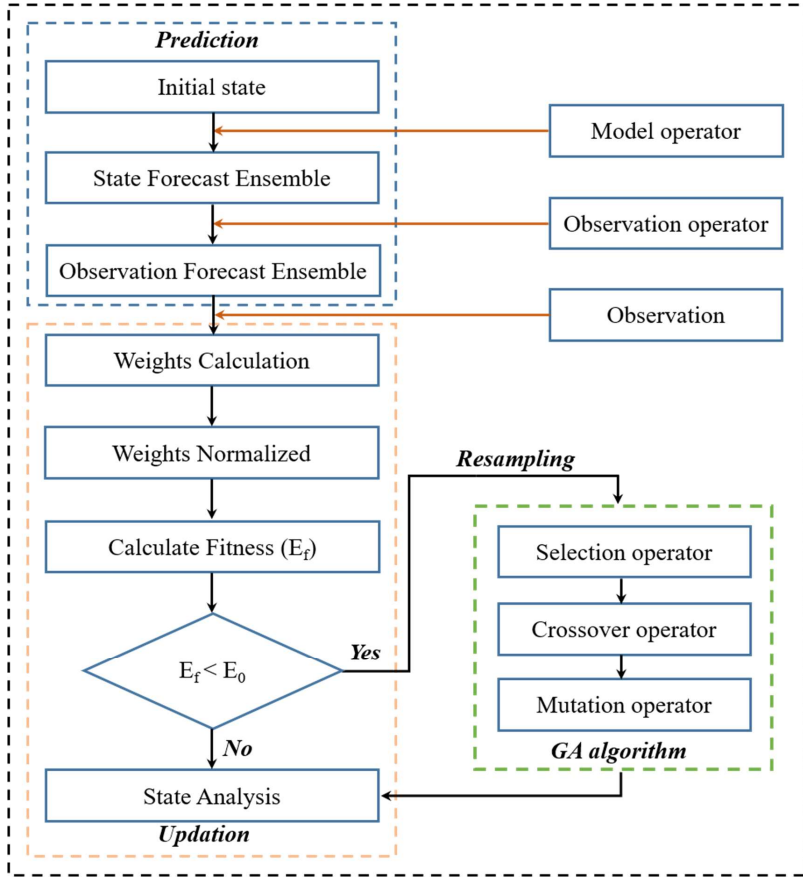
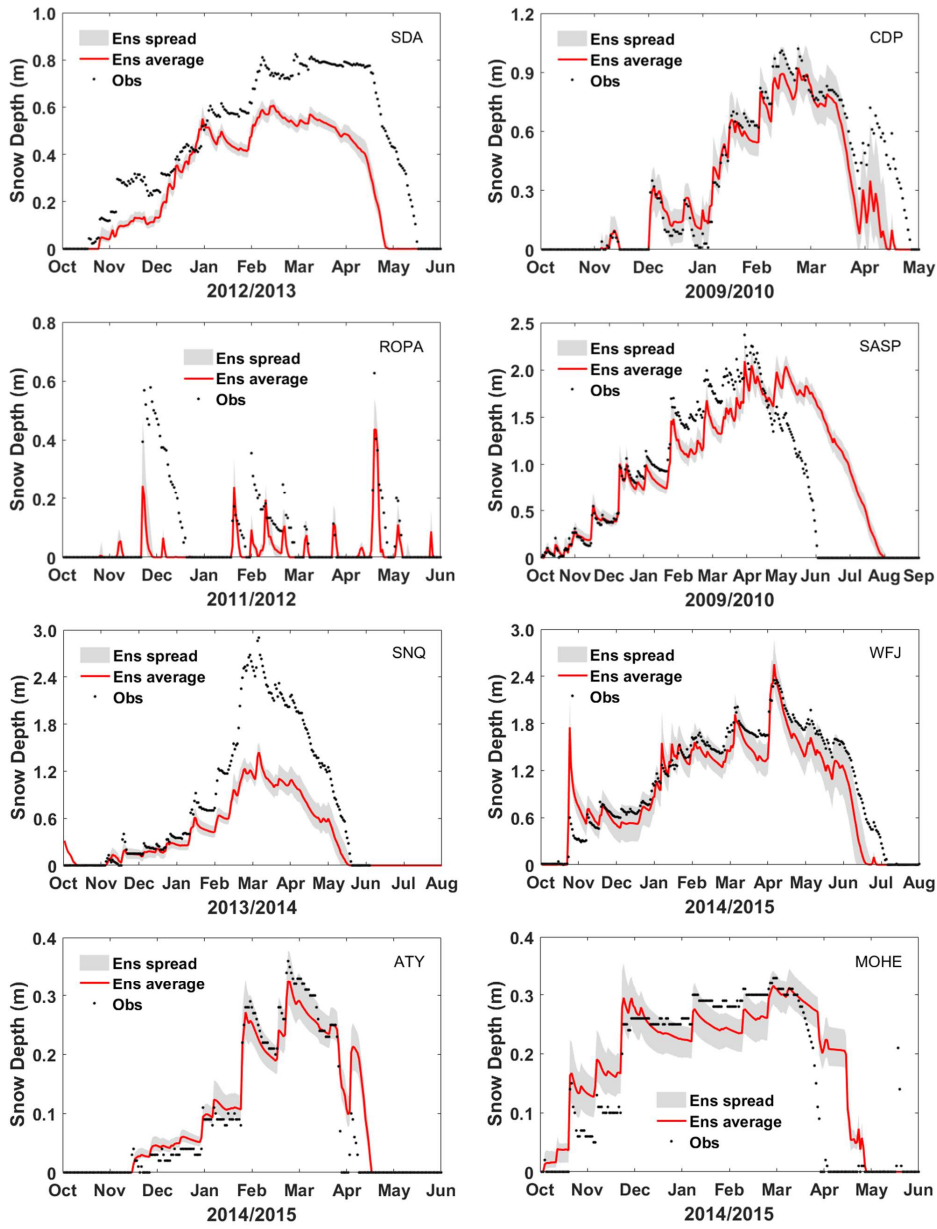


Figure 1. Flowchart of Genetic particle filter

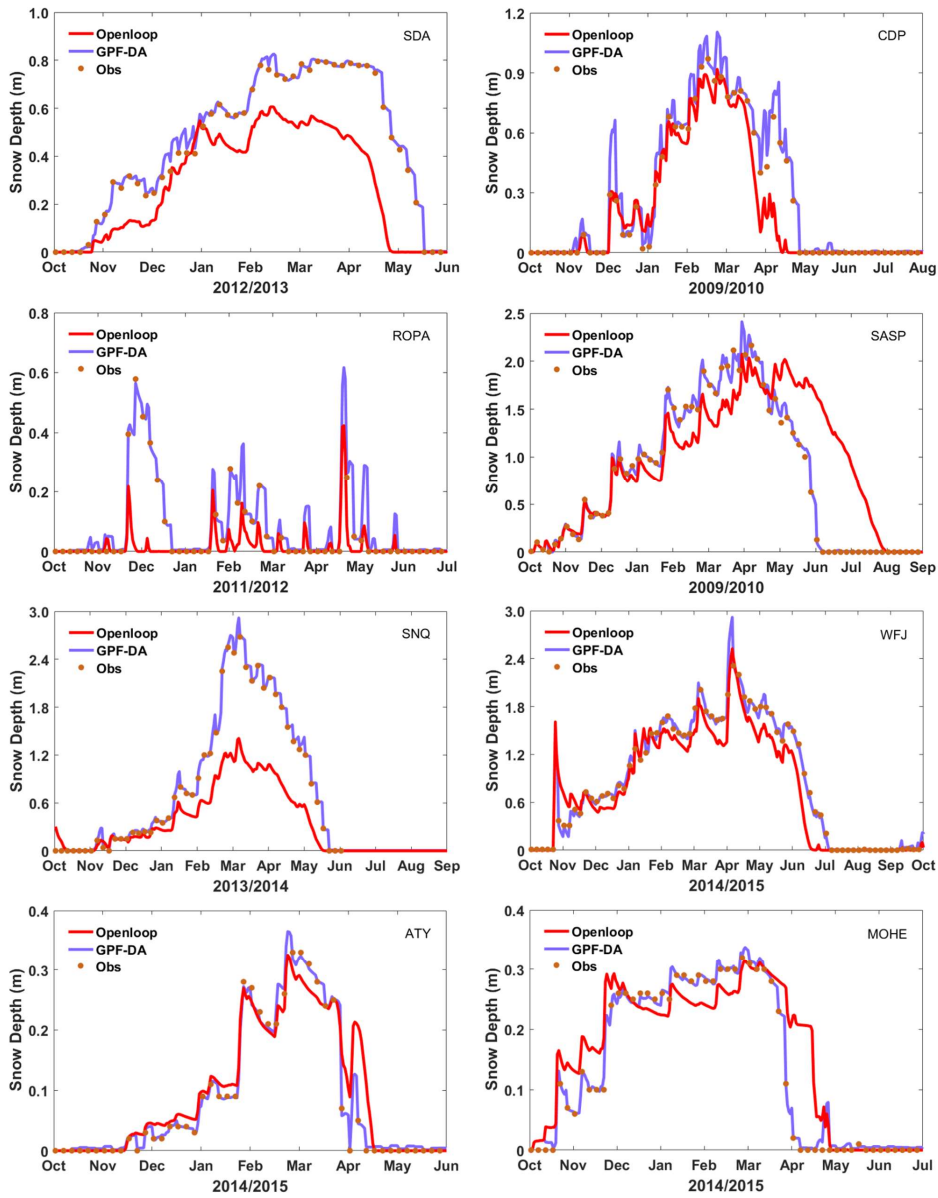
864

865

866



867  
868 **Figure 2.** Impact of the meteorological uncertainty on snow depth ensemble simulations  
869

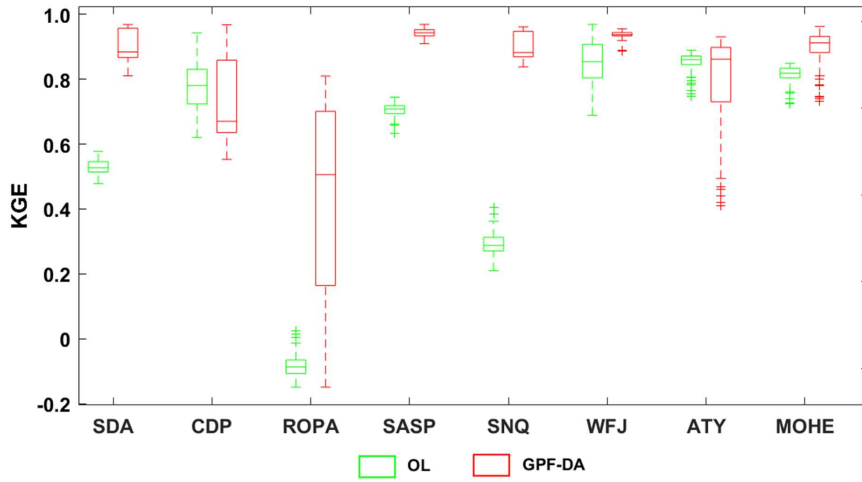


870

871 **Figure 3.** Evaluation of the SD at eight sites from mean ensemble simulation and assimilation with  
 872 the measurements.

873

874



875  
 876 **Figure 4.** The KGE values of SD simulations, the OL and GPF-DA are in green, red, respectively.  
 877 The bottom and top edges of each box indicate the 25th 75th percentiles, respectively. The line in the  
 878 middle of each box is the median.  
 879

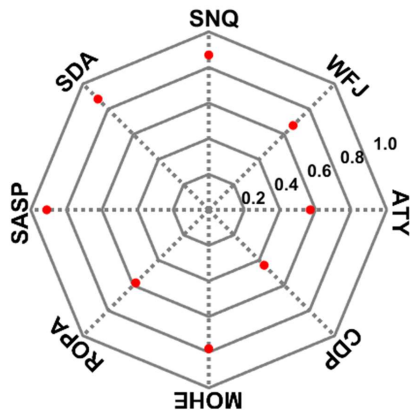
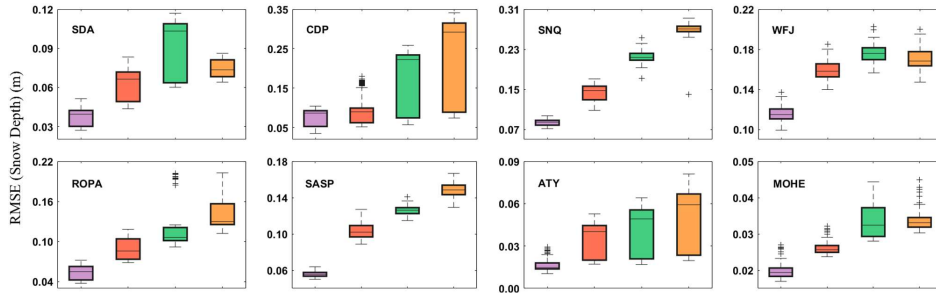


**Figure 5.** Comparison of the CRPSS value of GPF-DA at different sites.

880

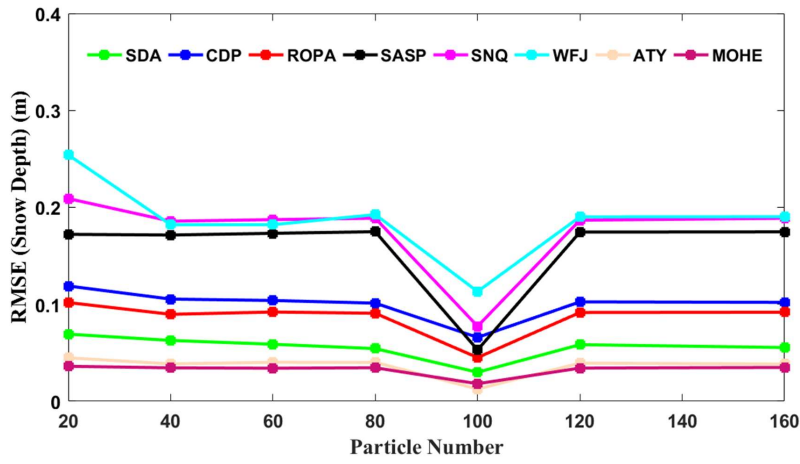
881

882



883  
 884 **Figure 6.** The RMSE values of SD simulations at different sites, from left to right in each subfigure  
 885 are the assimilation observation frequency is 5, 10, 15, 20 days, respectively, and with different colors.  
 886

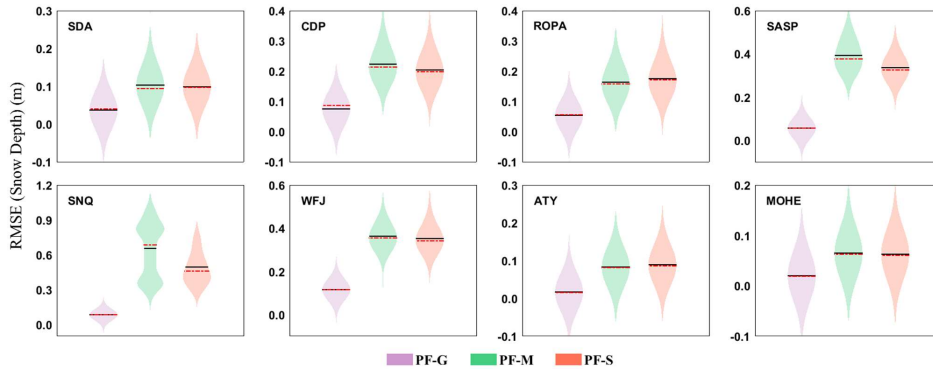




887

888 **Figure 7.** Sensitivity analysis of the GPF snow DA scheme to particle number at eight sites, during  
 889 different snow periods.

890



891

892 **Figure 8.** The RMSE values of SD simulations by three different resampling methods. For each  
 893 subfigure, from left to right are the particles resampled by genetic algorithm, multinominal method,  
 894 systematic method, respectively, and with different colors, the black line indicates the mean, and the  
 895 red line indicates the median; the kernel bandwidth was 0.05.

896